Hindawi
International Journal of Aerospace Engineering
Volume 2024, Article ID 3503468, 13 pages
https://doi.org/10.1155/2024/3503468

Research Article

An Iterative Determination Method of an Axial Deployment Force of a Lanyard-Deployed Coilable Mast in Local Coil Mode

Yu Liu,[1] **Liang Sun**,[1] **Hai Huang**,[1] **Xurui Zhao**,[2] **Jiahao Liu**,[1] **and Yishi Qiao**[3]

[1]*School of Astronautics, Beihang University, 37 Xueyuan Rd., Beijing 100191, China*
[2]*Institute of Remote Sensing Satellite, China Academy of Space Technology, 104 Youyi Rd., Beijing 100094, China*
[3]*Satellite Engineering Department, China Siwei Surveying and Mapping Technology Co. Ltd., 65 Zhichun Rd., Beijing 100190, China*

Correspondence should be addressed to Liang Sun; sunliang@buaa.edu.cn

Received 7 May 2022; Revised 26 September 2023; Accepted 27 January 2024; Published 26 March 2024

Academic Editor: Antonio Concilio

The axial deployment force is an indispensable parameter of a lanyard-deployed coilable mast, which reflects its load capacity in practical applications. However, research on the axial deployment force in the literature is very limited, and there are no mature numerical methods to determine this parameter in the design stage of coilable masts. In this paper, a numerical method for determining the axial deployment force of a lanyard-deployed coilable mast in the local coil mode is presented. Through this method, the designer can quickly obtain the estimated value of the axial deployment force in the design stage, which is convenient for the quantitative design of parameters. To verify the correctness of the proposed method, a dynamic simulation of the coilable mast is carried out, and a microgravity test is performed. The comparison results show that the error between the numerical method and the simulation and experimental results is less than 5%, which proves the correctness of the proposed method. In addition, the coilable mast studied in this paper has been verified by an actual microsatellite deployment in orbit.

1. Introduction

Compared with traditional large satellites, microsatellite technology has been rapidly developed in recent years because of its advantages of light weight, small size, and low cost. However, the small size limits the application of microsatellites. A feasible way to solve this problem is to change the structure of the microsatellites. Then, high-precision space exploration is achieved by removing the payload away from the microsatellite platform [1–3]. A deployable mechanism [4–6], such as a coilable mast, is usually used. A coilable mast is a one-dimensional deployable mechanism consisting of three consecutive longerons and a series of transverse battens and diagonal cables. It possesses the merits of a high packing factor, light weight, and simple structure.

The coilable mast can be deployed in three ways, including free deployment, lanyard deployment, and nut deployment. Lanyard deployment is a passive deployment mode in which a lanyard is used to control the deployment speed and stability. At the same time, lanyard deployment consists of two methods: the helix mode and local coil mode. In most cases, the local coil mode is preferable because the coilable mast has a higher stiffness against lateral forces during deployment. Therefore, the lanyard-deployed coilable mast in the local coil mode is the most suitable for microsatellite applications.

The axial deployment force is an indispensable parameter of a lanyard-deployed coilable mast, which reflects the load capacity of the coilable mast and has guiding significance for the design of dampers or motors controlling the deployment process. At present, it is inevitable to determine the axial deployment force through complex simulations and prototype tests. Therefore, establishing a numerical method that can accurately estimate this parameter is convenient for developing designs. However, research on the determination of the axial deployment force is limited. Natori et al. listed three types of simplex masts and observed and compared the longeron deformation under different axial deployment forces [7]; however, they only performed

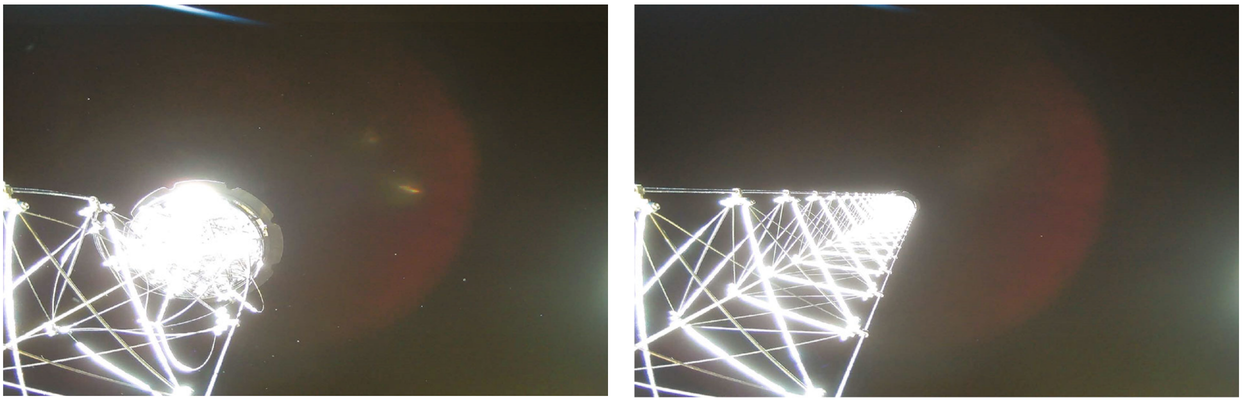

(a) (b)

Figure 1: Images of coilable mast in space: (a) during deployment; (b) after deployment.

a qualitative analysis and did not quantitatively determine the value of the axial development force. Kitamura et al. studied a Y-section hingeless mast and determined an empirical formula for the axial deployment force of the coilable mast in local coil mode [8]. Although they found that the axial deployment force was affected by the stiffness and structure of the coilable mast, it is difficult to obtain the stiffness of the coilable mast through complex simulations and tests at the design stage due to the strong nonlinearity and rigid-flexible coupling characteristics.

In this paper, a numerical method for determining the axial deployment force of a lanyard-deployed coilable mast in the local mode is presented. With this method, the axial deployment force can be quantified without knowing the stiffness of the coilable mast in advance, thus avoiding complicated simulation and testing. The aim of the numerical calculation method proposed in this paper is to determine the axial deployment force of a coilable mast through the longeron deformation of the transition zone. The "standard shape" of the longeron deformation in the transition zone is defined. The three continuous longerons are simplified into thin elastic rods that satisfy the cylindrical constraint hypothesis [9, 10]. Then, the force and deformation of the thin elastic rods are analysed by using Kirchhoff dynamic analogy theory [11]. The axial deployment force of the coilable mast conforming to the "standard shape" of the longeron deformation of the transition zone can be obtained.

In Section 2, the numerical method to determine the axial deployment force of a lanyard-deployed coilable mast in the local coil mode is described in detail. In Section 3, dynamic simulations of the deployment and microgravity deployment test are carried out. In Section 4, the correctness of the proposed method is verified, and the results are verified and discussed.

It is worth emphasizing that the research object of this paper has been applied in practice. On October 14, 2021, the SSS-1 satellite (30 kg) developed by Beihang University was successfully launched into space. The coilable mast studied in this paper was installed and deployed on October 16, 2021. A space camera is installed at the bottom to record the deployment process, as shown in Figure 1. The length of the coilable mast is approximately 2 metres, and its weight is 0.8 kg. In addition, the packing factor can reach 20/1. Undoubtedly, it lays a solid foundation for the subsequent in-orbit application of coilable masts.

2. Numerical Determination Method of the Axial Deployment Force

Under lanyard control, the deployment speed of a lanyard-deployed coilable mast is approximately constant. In this way, the axial deployment force and the lanyard tension can be considered balanced. The method proposed in this paper can be used to obtain the axial deployment force by solving the lanyard tension of the coilable mast. By analysing the deformation of the longeron in the transition zone, the lanyard tension can be determined.

As shown in Figure 2, in the local coil mode, the transition zone is located between the deployed zone and the coiled zone of the lanyard-deployed coilable mast. During deployment, the shape in the transition zone changes periodically within a small range, which results in small periodic fluctuations in the lanyard tension. To obtain the estimated value of the lanyard tension, the "standard shape" in the transition zone is defined in this paper according to the experiment, and the lanyard tension corresponding to this shape is what we need to solve. The actual lanyard tension and axial deployment force will fluctuate in a small range around this value.

2.1. Definition of the "Standard Shape" in the Transition Zone. According to previous research and development tests of coilable masts, the number of segments in the transition zone is approximately 4. As shown in Figure 3, the segments are defined as segments 1 to 4, the corresponding longerons are defined as rods 1 to 4, and the battens are defined as battens 1 to 5.

To quantitatively define the "standard shape" in the transition zone, the helical angle θ of the longeron, which is defined as the angle between the normal direction of the longeron cross section and the deployment direction of the coilable mast, is introduced as shown in Figure 4. In the deployed zone, the longeron is in a state of full deployment, and the helical angle is $\theta_{\text{deploy}} = 0^{\circ}$. In the coiled zone, the

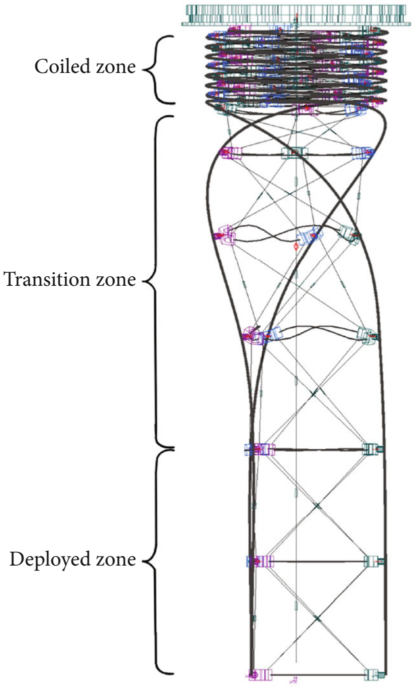

Figure 2: Coilable mast in local coil mode.

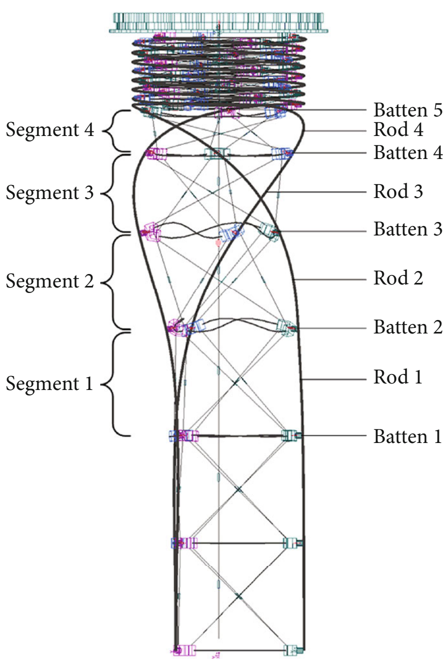

Figure 3: "Standard shape" of transition zone.

longeron is in a uniform helical state, satisfying the cylindrical constraint, as shown in Figure 5, and points A and B represent two adjacent hinges in one longeron. In cylindrical triangle ABC, the helical angle is $\theta_{\text{coil}} = \arccos(h_1/t)$, where t and h_1 are the pitch length and the height between two adjacent hinges, respectively. Combined with the definition of the helical angle, the "standard shape" in the transition zone can be quantitatively defined such that the helical angle

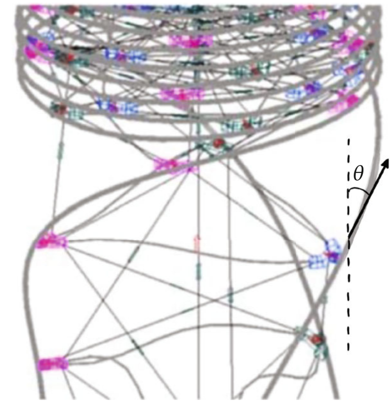

Figure 4: Definition of helical angle θ.

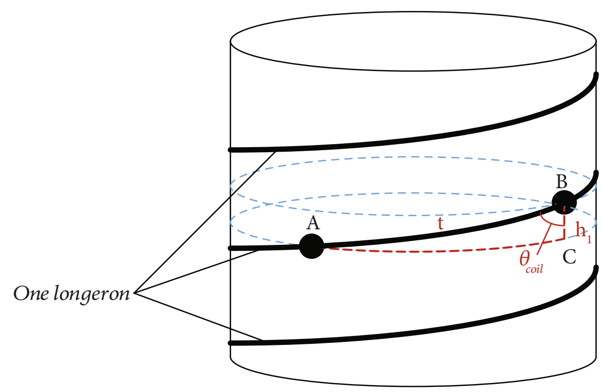

Figure 5: Helical angle in coiled zone θ_{coil}.

of the longeron increases from θ_{deploy} to θ_{coil} in 4 segments. The selection of the helical angle θ to describe longeron deformation is based on three considerations. The first is that the helical angle θ is an intuitive physical parameter that visualizes the deformation shape. The second is that this parameter can be solved quantitatively by the deformation equation extended from Kirchhoff's kinetic analogy theory, which will be introduced in detail in the following sections. The third is that when the helical angle θ is determined, the remaining geometric parameters are properly known based on geometric constraints, so as to completely describe longeron deformation.

It should be noted that in the transition zone of the coilable mast, the battens buckle under pressure, resulting in a slight reduction in the coiled radius of the longerons in the transition zone. However, this reduction can be ignored because it is small relative to the coiled radius. Therefore, it can be assumed that the longeron of the coilable mast deforms along the cylinder in the transition zone, and the cylindrical radius is the coiled radius [12].

2.2. Equations of the Longeron Deformation. In this section, based on Kirchhoff dynamic analogy theory, a deformation equation is introduced to describe the relationship between the deformation of a longeron and the external load. This equation is the basis of the deformation analysis of longerons in the transition zone.

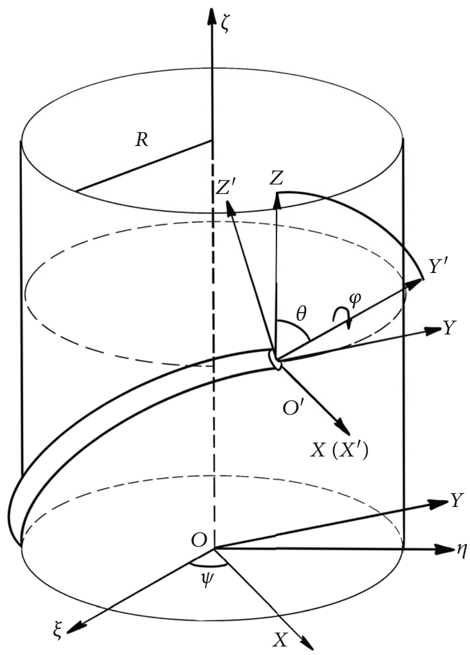

Figure 6: Definition of coordinate systems.

First, we need to establish a series of coordinate systems. As shown in Figure 6, in the rectangular coordinate system, $O\zeta$ is the central axis of the cylinder, and $O\xi$ is randomly defined along the cross section of the cylinder. The coordinate system $O\xi\eta\zeta$ is rotated about the $O\zeta$ axis by ψ to obtain the coordinate system $OXYZ$. Then, $OXYZ$ is translated from O to the center point of the rod cross section O'. Finally, the coordinate system $O'XYZ$ around $O'X$ is rotated by $(\pi/2) - \theta$ to obtain the coordinate system $O'X'Y'Z'$.

φ is taken as the angle around the axis $O'Y'$, representing the rotation between two adjacent cross sections of the rod. The angles ψ, θ, and φ are selected to describe the position and orientation of the rod cross section. All are functions of the arc length s. $d\psi/ds$, $d\theta/ds$, and $d\varphi/ds$ along the arc length describe the deformation of the rod. $d\psi/ds$ and $d\theta/ds$ define the changes in the rotating angles around the $O'Z$ and $O'X$ axes, respectively, between the adjacent cross sections, and $d\varphi/ds$ describes the change in the torsion angle between the adjacent cross sections. Under the cylindrical constraint assumption, $\psi(s)$ and $\theta(s)$ satisfy

$$d\psi = \frac{ds \cdot \sin\theta}{R}. \tag{1}$$

Then, according to Kirchhoff's kinetic analogy theory, the longeron with an external load on both ends satisfies the following deformation equation when the dynamic effect of the mass deployment and the reduction of the coiling diameter in the transition zone are ignored.

$$\frac{d^2\theta}{ds^2} = -\frac{1}{R}(l_0\cos\theta - m\cos 2\theta) + \left(\frac{p}{2} + \frac{2\cos\theta\sin^2\theta}{R^2}\right)\sin\theta. \tag{2}$$

In Equation (2), R is the coiling radius, s is the arc length of the thin elastic rod, and θ is the helical angle of the thin elastic rod at the current cross section. p, l_0, and m are integral constants. Here, p is proportional to the force acting axially on the rod cross section along the $O'Z$ axis. l_0 is proportional to the torque on the $O\zeta$ axis; and m is related to the torsional deformation. The specific equations are as follows:

$$\begin{cases} l_0 = \dfrac{M_0}{A} = \dfrac{F_Y R + M_Z}{A} = \left(\dfrac{R}{A}\right)F_Y + m\cos\theta + \dfrac{\sin^3\theta}{R}, \\ m = \dfrac{C}{A}\omega, \\ \omega = \dfrac{d\psi}{ds}\cos\theta + \dfrac{d\varphi}{ds}, \\ p = \dfrac{2F_Z}{A}. \end{cases} \tag{3}$$

In Equation (3), A and C are the bending and torsional stiffness of the cross section, respectively, which are related to the material properties of the longeron. M_0 and M_Z are the external torques of the cross section along the $O\zeta$ axis and the $O'Z$ axis, respectively. F_Y and F_Z are the external forces of the cross section along the $O'Y$ axis and the $O'Z$ axis, respectively. ω is the torsional curvature of the longeron, which remains constant along the arc length, while the rod is constrained only at both ends [11]. Then, Equation (4) can be obtained as follows:

$$\int_0^t \omega ds = \int_0^t \left(\frac{d\psi}{ds}\cos\theta + \frac{d\varphi}{ds}\right) ds = \omega t. \tag{4}$$

According to the actual assembly conditions of the longeron of the coilable mast, the torsion of the longeron between the adjacent hinges is limited. Thus, in the interval $[0, t]$, $d\varphi/ds$ is equal to 0. Combined with Equation (1), the relationship between the helical angle and torsion ratio can be obtained as follows:

$$\begin{aligned} \omega t &= \int_0^t \left(\frac{d\psi}{ds}\cos\theta + \frac{d\varphi}{ds}\right) ds = \int_0^t \left(\frac{d\psi}{ds}\cos\theta\right) ds + \int_0^t \frac{d\varphi}{ds} ds \\ &= \int_0^t \frac{\sin\theta\cos\theta}{R} ds. \end{aligned} \tag{5}$$

2.3. Deformation Analysis of the Longeron in the Transition Zone. In this section, the method of solving the deformation equation in Section 2.2 will be introduced in detail, and the deformation analysis of the longeron in the transition zone will be carried out. Due to the internal load caused by transverse battens and diagonals, the equation established in the above section cannot be directly used to solve the entire deformation in the transition zone. One feasible approach is to discretize the transition zone into several parts, as shown in Figure 4. In this way, each discrete rod satisfies the conditions of the previous deformation equation, and the deformation in the transition zone can be obtained by solving the deformation from rod 4 to rod 1 in turn. The upper end of each rod is where the arc length is $s = 0$, and the lower end is where $s = t$.

To solve Equation (2) for each rod, it is necessary to determine the integral initial values $\theta_i(0)$ and $d\theta_i(0)/ds$ and the integral constants p_i, l_{0i}, and m_i ($i = 1,2,3,4$), which are related to the boundary conditions and external forces of each rod.

First, we need to determine the initial value of the integral. According to the definition of the "standard shape", the initial value of $\theta_4(0)$ is equal to θ_{coil}. To simplify the calculation, a reasonable assumption is made on the longeron deformation in transition zone based on the results of simulations and tests. It is considered that the helical angle of the longeron in segment 1 is maintained as $\theta_{\text{deploy}} = 0°$, and the helical angle of the longeron in segments 2-4 presents a linear change relationship, which is expressed by Equation (6) [13]. The purpose of this assumption is only to estimate the initial integral values $\theta_4(0)$ and $d\theta_4/ds_{s=0}$ of segment 4 to make the deformation equation solvable, and it will not affect the solution of the nonlinear state regions of the helical angle.

$$\begin{cases} \theta_4(0) = \theta_{\text{coil}}, \\ \left.\dfrac{d\theta_4}{ds}\right|_{s=0} = \dfrac{\theta_{\text{deploy}} - \theta_{\text{coil}}}{3t}. \end{cases} \tag{6}$$

Since the deformation of the longeron in the transition zone is continuous, in segment 3 to segment 1, according to Liu's research [11], the helical angle and its rate satisfy Equation (7). Combined with Equations (6) and (7), the initial integral value required for each rod can be obtained.

$$\begin{cases} \theta_i(0) = \theta_{i+1}(t), \\ \left.\dfrac{d\theta_i}{ds}\right|_{s=0} \left(m_i - \dfrac{3}{2R} \sin 2\theta_i(0) \right) = \left.\dfrac{d\theta_{i+1}}{ds}\right|_{s=t} \left(m_{i+1} - \dfrac{3}{2R} \sin 2\theta_{i+1}(t) \right). \end{cases} \tag{7}$$

The second step is to determine the integral constant of each rod. According to Equation (3), to determine the integral constants p_i, l_{0i}, and m_i, we need to identify F_{Zi}, M_{0i}, and F_{Yi}. These forces and torques can be determined by boundary force analysis. As shown in Figure 6, considering the segments and the coiled zone on rod i as a whole T, T is in an equilibrium state with the lanyard tension F_L, the rod reaction force and torque, and the diagonal cable tension. F_{ri}, F_{vi}, and F_{hi} are three components of the diagonal cable tension. Thus, the forces and torques are balanced along the $O\zeta$ axis to satisfy Equation (8). It should be noted that the coilable mast is a spatially axisymmetric structure, so the force analysis of only one longeron is shown in Figure 7, and the forces and torques of the other two longerons on T are the same.

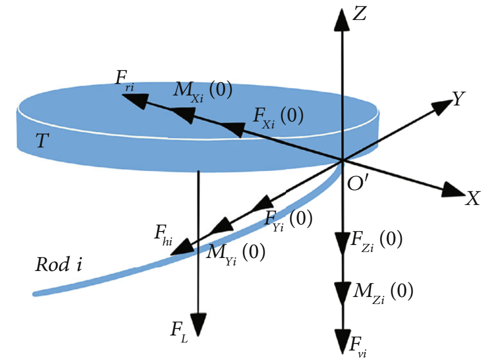

FIGURE 7: Equilibrium analysis of the unity T.

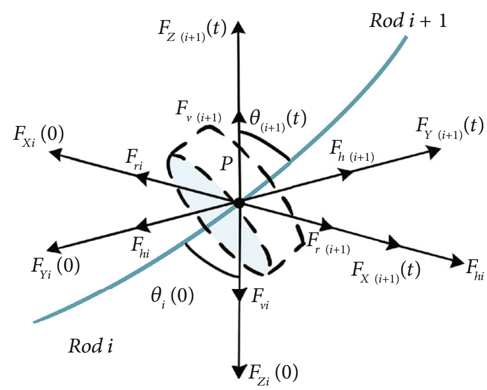

FIGURE 8: Infinitesimal balance analysis.

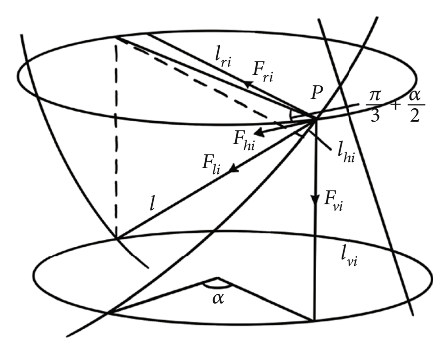

FIGURE 9: Section deformation analysis.

$$\begin{cases} F_L + 3F_{Zi}(0) + 3F_{vi} = 0, \\ 3(F_{Yi}(0)R + M_{Zi}(0) + F_{hi}R) = 0. \end{cases} \tag{8}$$

The infinitesimal at the connection point between the adjacent rods is considered the object of analysis, as shown in Figure 8. Ignoring dynamic effects, the force is balanced

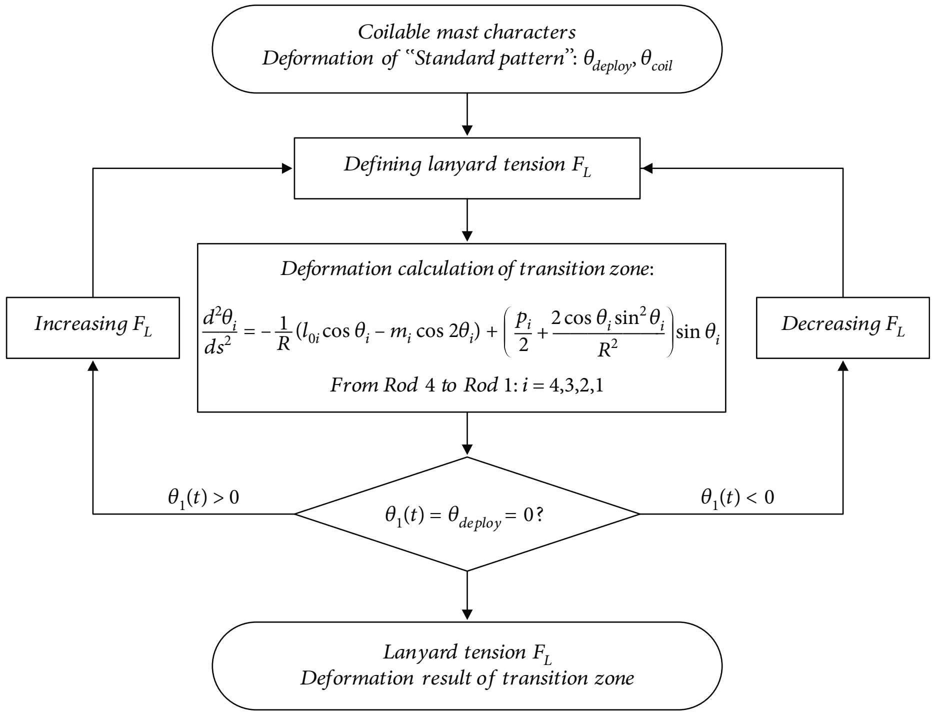

Figure 10: Deformation analysis process for calculating the lanyard tension.

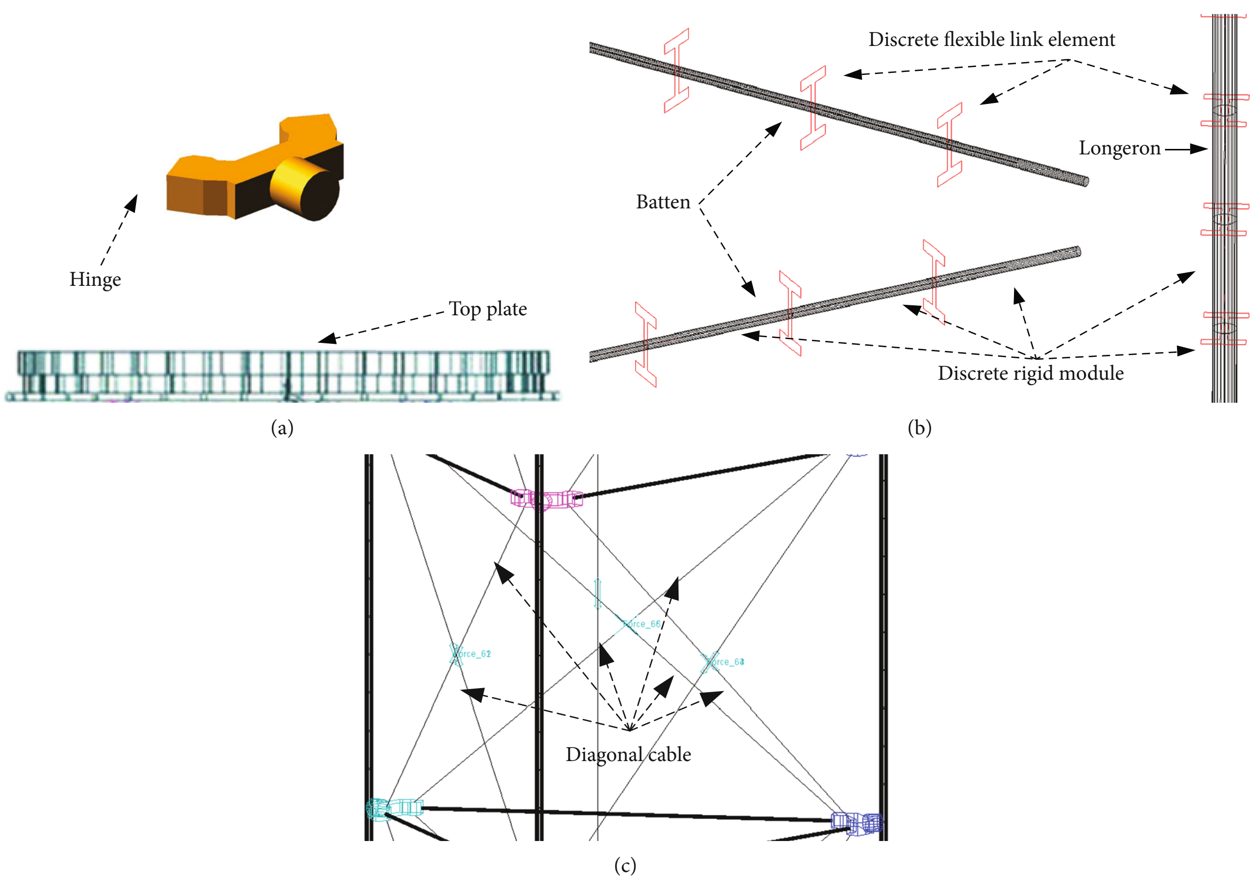

Figure 11: Model of different components: (a) rigid body; (b) flexible body; (c) force.

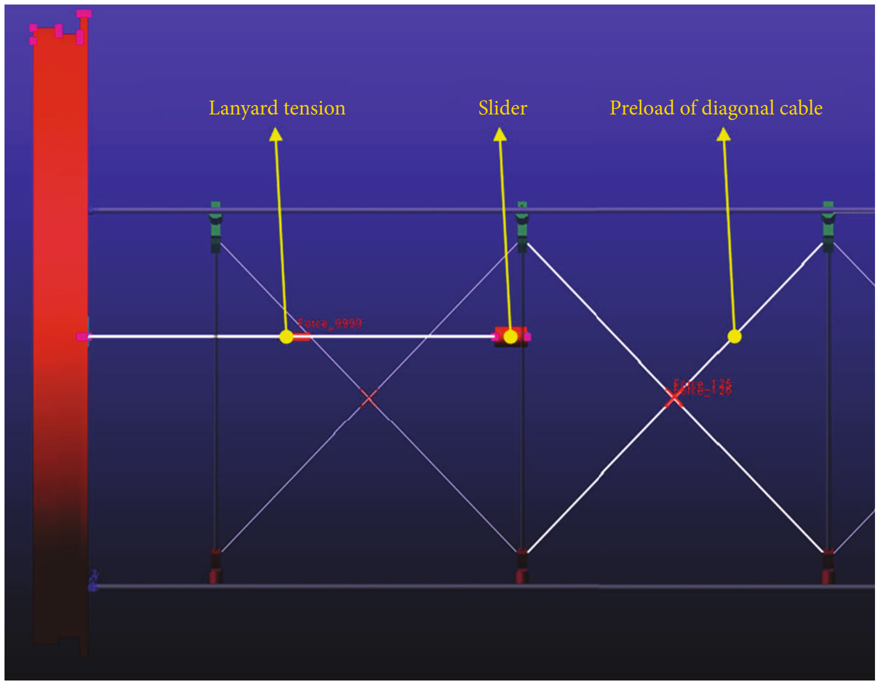

FIGURE 12: Lanyard tension and diagonal cables in the simulated model.

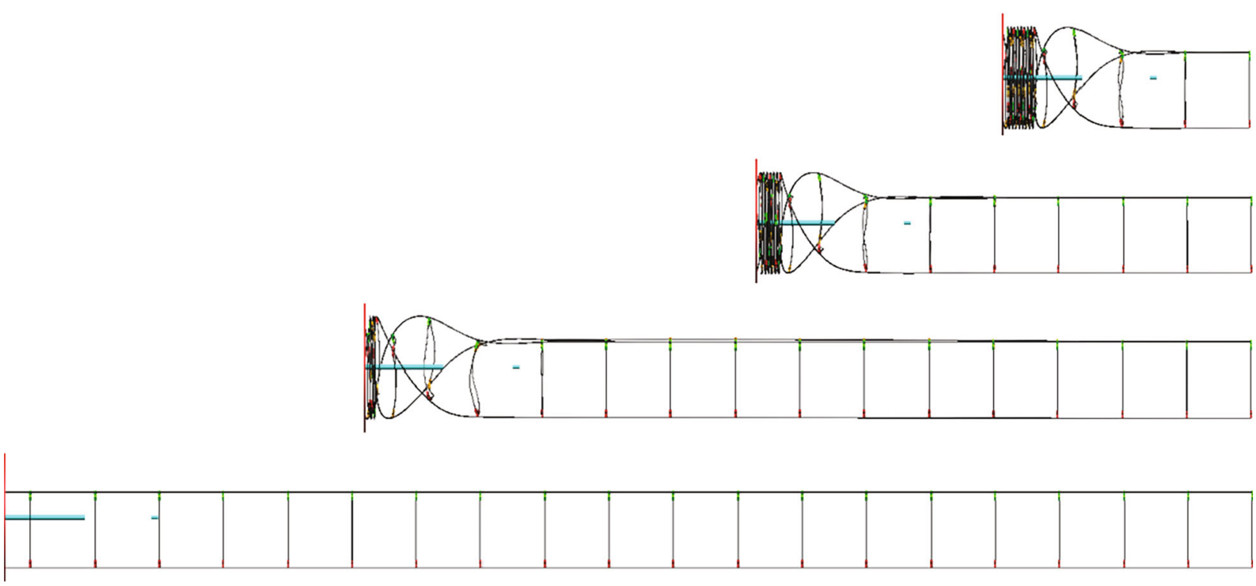

FIGURE 13: Virtual prototype model of coilable mast.

along the $O'Y$ and $O'Z$ axes, satisfying Equation (9). $F_{Z(i+1)}(t)$ and $F_{Y(i+1)}(t)$ can be solved by p_{i+1} and l_{0i+1}.

$$\begin{cases} F_{Yi}(0) + F_{hi} = F_{Y(i+1)}(t) + F_{h(i+1)}, \\ F_{Zi}(0) + F_{vi} = F_{Z(i+1)}(t) + F_{v(i+1)}. \end{cases} \quad (9)$$

In the experiment, it was observed that the diagonal cables of segments 4 and 3 in the transition zone of the coilable mast were not tensioned. Equations (8) and (9) can be simplified because F_{hi} and F_{vi} are equal to 0. F_{Zi}, M_{0i}, and F_{Yi} can be calculated easily. However, for segments 2 and 1, the function of the diagonal cable tension must be considered. Therefore, more equations need to be added to calculate the diagonal cable tension. According to the segment deformation analysis shown in Figure 9, the tension component of the diagonal cable can be obtained. Assuming the length of the diagonal cable is l, the three components in $O'XYZ$ are l_{ri}, l_{hi}, and l_{vi}. Since diagonal cables only withstand tension, the diagonal cable tension components F_{ri},

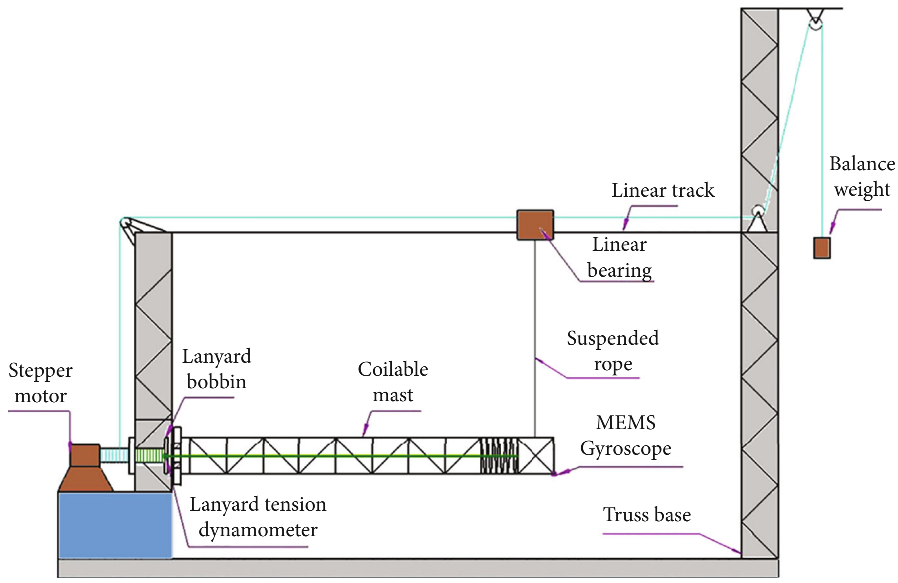

Figure 14: Microgravity deployment test system.

F_{hi}, and F_{vi} have the same geometric relationship to the diagonal cable length. Therefore, the diagonal cable tension can be calculated from Equation (10).

$$\begin{cases} \dfrac{F_{li}}{l} = \dfrac{F_{hi}}{l_{hi}} = \dfrac{F_{vi}}{l_{vi}} = \dfrac{F_{ri}}{l_{ri}}, \\ l_{vi} = \displaystyle\int_t \cos\theta_i ds, \\ \alpha_i = \displaystyle\int_t \dfrac{\sin\theta_i}{R} ds, \\ l_{hi} = 2R\cos\left(\dfrac{\pi}{3} + \dfrac{\alpha_i}{2}\right)\sin\left(\dfrac{\pi}{3} + \dfrac{\alpha_i}{2}\right), \\ l_{ri} = 2R\sin^2\left(\dfrac{\pi}{3} + \dfrac{\alpha_i}{2}\right), \\ l = \sqrt{\left(l_{vi}^2 + l_{hi}^2 + l_{ri}^2\right)}. \end{cases} \tag{10}$$

Combined with Equations (6)–(10), all the initial values of the integral and the integral constants p_i, l_{0i}, and m_i for any rod i can be determined. When the characteristics of the coilable mast, including geometric dimensions and material properties, are given, the only unknown parameter in the deformation equation (Equation (2)) is the lanyard tension F_L. Therefore, as long as the lanyard tension F_L is given, the deformation equation from rod 4 to rod 1 can be solved in turn, and the deformation in the transition zone corresponding to the lanyard tension can be obtained.

Due to the strong nonlinearity of the deformation equation, the equation cannot be solved directly by the analytical solution, so the iterative calculation approach is a simple and effective method. The iterative solving process is shown in Figure 10. In the iterative solution process, the input parameters of the solution process mainly include two types: one is the characteristics of the coilable mast, including geometric dimensions and material properties, and the other is the parameters of the "standard shape" in the transition zone, θ_{deploy} to θ_{coil}. Then, the initial value of the lanyard tension F_{L0} is given, and the deformation in the transition zone is solved according to the deformation equation in Section 2.2. Then, the helical angle at the bottom of the transition zone $\theta_1(t)$ is compared with θ_{deploy}. If they are equal, it indicates that the transition zone has formed a "standard shape" and that the current lanyard tension is what we need. Then, the axial deployment force is obtained. If they are not equal, the deformation analysis will be repeated after adjusting the lanyard tension value until the transition zone forms a "standard shape."

Moreover, according to formula analysis and accumulated rich data of deployment simulations and tests of coilable masts with different configurations and dimensions, the relationship between the helical angle in the bottom of transition zone $\theta_1(t)$ and the lanyard tension is deeply explored, and they are found to be monotonic over a wide range. In other words, the system has strong stability to the initial value. More than that, the rich data of deployment simulations and tests can guide the selection of the initial value of the lanyard tension closer to the real value, which is conducive to improve the convergence speed of the system.

Remark 1. It should be noted that there are many kinds of uncertainties in application, including internal or external, parametric or nonparametric, constant, characteristic, or random. In a coilable mast, the uncertainties relate to geometric dimensions and material properties. For geometric dimensions, the uncertainties of the coiling radius and the batten pitch length are mainly caused by the assembly error of the coilable mast. For material properties, the uncertainties are mainly caused by material defects and degradation under large deformation. A comparison between the tests and simulations shows that the uncertainties do not cause large deviations in real-time applications.

(a)

(b)

FIGURE 15: Test platform: (a) front view; (b) side view.

Remark 2. It should be noted that in real engineering problems, there are complex systems whose structures, uncertain properties, and all the parameters are unknown. In this case, advanced system identification and signal processing approaches can be developed and optimized with sophisticated approaches [14]. This should be the focus of further research in this paper.

3. Deployment Dynamic Simulation and Microgravity Deployment Test

Through dynamic simulation and microgravity testing of the deployment process, the correctness of the numerical method is verified in Section 2.

3.1. Deployment Dynamic Simulation. The deployment simulation was carried out using MSC.ADAMS and based on the finite element method (FEM). The FEM is a general numerical method for solving partial differential equations in two or three space variables, which is a well-known and widely applied approach in almost every part of such engineering problems. To solve a problem, the FEM subdivides a large system into smaller, simpler finite elements which is achieved by a particular discretization in the space dimension. The simple equations that model these finite elements are then assembled into a larger system of equations that models the entire problem. The FEM approximates the unknown analytical equations over the domain and improves the approximation accuracy by minimizing an associated error function via the calculus of variations. As a complex rigid-flexible hybrid mechanism, the coilable mast is composed of components with different characteristics which will be introduced in the following paragraph, and the deployment process of the mast is strongly nonlinear due to the existence of mechanism clearance and large deformation of flexible components. So it is almost impossible to establish analytical equations of the problem and solve it accurately. Therefore, the FEM is an effective and necessary method for deployment simulation of the coilable mast [5, 15].

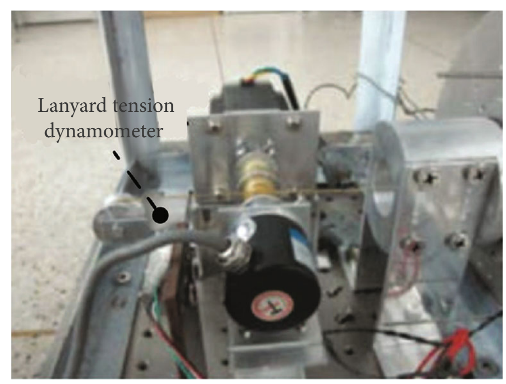

FIGURE 16: Lanyard tension dynamometer.

TABLE 1: Technical parameters of the coilable mast.

Parameter	Value
Coiling radius (R)	75 mm
Radius of longeron	1 mm
Radius of batten	0.65 mm
Batten pitch length (t)	95 mm
Height between hinges (coiled zone) (h_1)	3 mm
Material of hinge	Aluminum alloy Young's modulus: 70.6 GPa; Poisson's ratio: 0.33
Material of longeron and batten	Ti-Ni alloy Young's modulus: 83 GPa; Poisson's ratio: 0.31

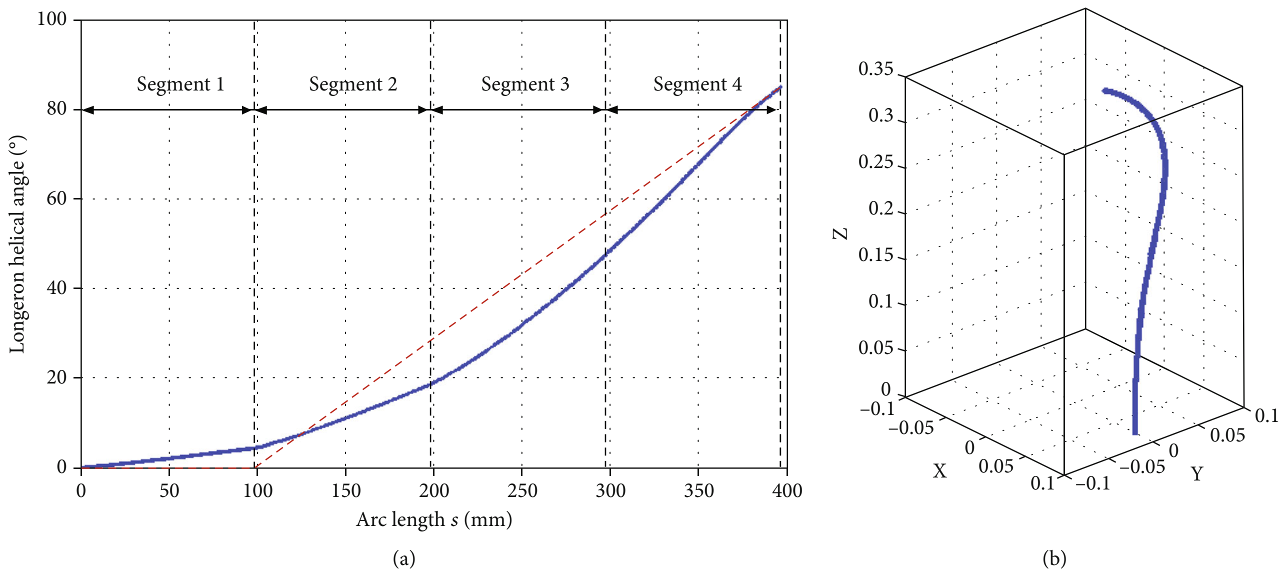

Figure 17: Longeron deformation in the transition zone: (a) helical angle; (b) longeron deformation.

As described in the previous paragraph, different components of the coilable mast exhibit different physical characteristics under applied loads. In this case, four modelling methods are used to reflect its deployment motion characteristics: (1) rigid body: the hinge and top plate of the coilable mast have little deformation during the process and can be simplified into rigid units; (2) flexible body: for longerons and battens, because they are thin rods with elasticity, they will undergo large deformation during the deployment process and are considered flexible bodies. In particular, the longerons and battens are discretized into a series of rigid modules, and discrete flexible link elements are used to connect the adjacent rigid modules to simulate their deformation characteristics; (3) force: since the diagonal cable can only be tensioned but not compressed, a pair of actions and reactions is used to complete the modelling work. The direction of the force is along the central axis of the diagonal cable, and its value is related to the distance between the two ends; and (4) kinematic pair: the components in the simulation model are connected to each other, and the motion relationship is limited by several kinematic pairs, such as the rotating pair between the longeron and the top plate and the fixed pair between the hinge and the longeron. The modelling relationships of the different components are shown in Figure 11. In addition, a slider is set to control the deployment speed of the coilable mast, and the force between the top plate and the slider is the lanyard tension, as shown in Figure 12.

The simulation model of the coilable mast during the deployment process is shown in Figure 13. The deployment process takes place at a constant speed of 30 mm/s. The deformation in the transition zone is basically unchanged, consistent with the defined “standard shape.”

3.2. Microgravity Deployment Test. To simulate the weightless environment in space, a microgravity deployment test system for a coilable mast was developed, as shown in Figure 14. The truss base is fixed to the ground to provide mounting space for the coilable mast and support for all other equipment. The coilable mast is placed horizontally, and the top plate is connected to a sliding linear bearing by suspension rope. The linear bearing is located directly above the top plate, so the tension of the rope counteracts the gravity of the coilable mast, creating a microgravity environment. During the development process, as the top plate moves forward, the linear bearing must move synchronously along the linear trajectory to confirm that the suspension rope is in the direction of the plumb line. The lanyard bobbin and balancing weight are especially introduced. When the coilable mast is released by the stepper motor, the presence of the lanyard bobbin ensures that the deployment length of the coilable mast is equal to the movement length of the linear bearing, and in this process, the friction can be overcome by a balancing weight. The physical test platform is shown in Figure 15.

During the coilable mast deployment test, a tension dynamometer mounted on the bottom plate was used to measure the lanyard force with a sampling frequency of 5 Hz, as shown in Figure 16. In addition, the stepped motor is started to release the coilable mast at a speed of 30 mm/s, maintaining consistency with the dynamic simulation.

4. Result Validation and Discussion

4.1. Numerical Calculation Result of Axial Deployment Force. The coilable mast verified on the SSS-1 satellite is taken as the object. The characteristics of the coilable mast are shown in Table 1. According to the numerical method presented in Section 2, the axial deployment force of the coilable mast is calculated as 11.808 N. The helical angle change and longeron deformation in the transition zone are shown in Figure 17. The red-dotted line in Figure 17(a) is the assumption we made of helical angle to obtain the initial integral values, which is described in Section 2.3. This assumption

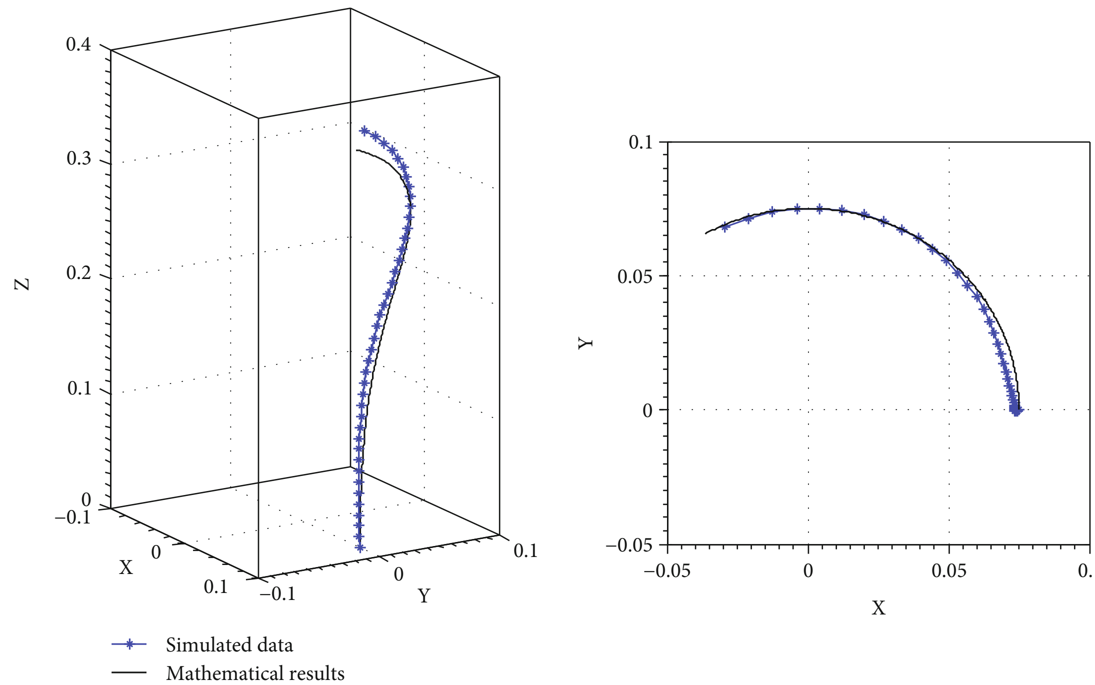

Figure 18: Deformation comparison between mathematical results and simulated data.

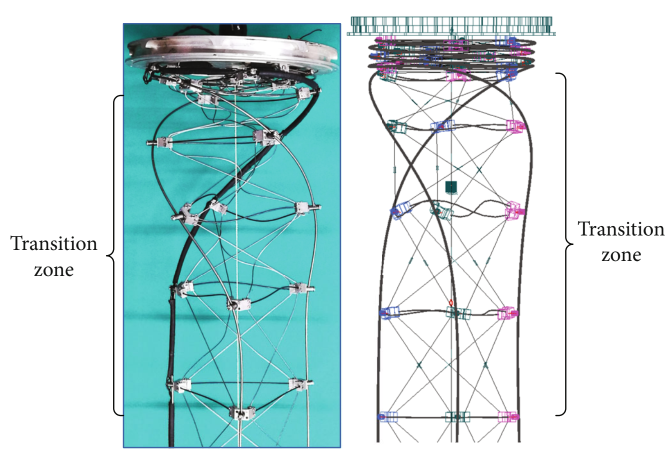

Figure 19: Longeron deformation comparison between tested results and simulated data.

can be considered to be a linear simplification of the actual helical angle. And the assumption does not affect the solution of the actual nonlinear regions of helical angle of the longeron.

In the transition zone, from bottom to top, the helical angle of the longeron changes from 0 to θ_{coil}. The change rate of the longeron helical angle of segment 3 and segment 4 along the arc length s is greater than that of segment 1 and segment 2. Due to the limitation of the diagonal cable, the torsional stiffness of segment 1 and segment 2 is greater than that of segment 3 and segment 4. Therefore, the longeron bearings of segment 1 and segment 2 are subjected to greater torsional stress, and the helical angle changes more slowly.

4.2. Validation of the Longeron Deformation. The longeron deformation can be used to determine the mechanical properties of the coilable mast, so it has been verified for the first time. The longeron deformation in the simulation has similar characteristics to the mathematical results, as shown in Figure 18. It is worth noting that the coiling radius near the bottom of the transition zone is slightly reduced in the simulation. This phenomenon is reasonable because the battens bend under the action of diagonal forces during the development process. Furthermore, the transition zone of the simulation model and the actual test model was compared, as shown in Figure 19. The simulation model can well reflect the actual deployment state of the coilable mast.

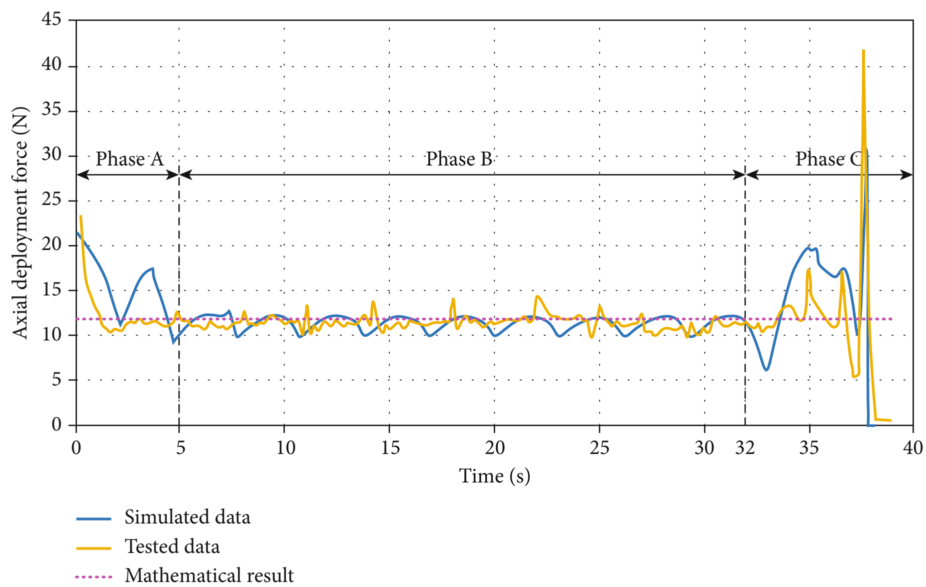

Figure 20: Axial deployment force variation during deployment process.

From the above comparison, it can be seen that the deformation analysis of the numerical method accords with the actual situation of the coilable mast.

4.3. Validation of Axial Deployment Force. According to the above numerical calculation method, the axial deployment force is 11.808 N. The corresponding microgravity test and dynamic simulation results are given. The comparison of the axial deployment force of the three methods is shown in Figure 20.

The development process of the coilable mast is divided into three phases. Phases A and C represent the beginning and end of the development, respectively, where the axial development force changes irregularly because the transition zone of the coilable mast has not yet fully formed or gradually disappeared. Phase B is the stable development phase, and the axial development force presents periodic fluctuations. By comparing the three results in phase B, it can be found that the numerical result is a constant value because it is obtained while ignoring the mast deployment dynamic effects, and both simulation and test results fluctuate periodically near the numerical results. The main reason for the periodic fluctuation of the axial development force is the reflection of energy conversion when a section is unrolled in the local coil mode, which can be called "snap through" [16]. At this moment, the deformation energy of longerons and battens is quickly transformed into the kinetic energy of the top plate, resulting in a sudden increase in the axial development force. Compared with the simulation results, the fluctuation of the test results is relatively irregular, which is mainly due to the influence of measurement noise and actual friction between the hinges of the coilable mast.

The quantitative comparison results of the axial deployment force in phase B are shown in Table 2. Because the axial deployment force in the simulation and test results fluctuates periodically in a small range, the average value is solved to compare with the numerical results. The average value of the simulation result and test results is slightly smaller than that of the numerical results. The reason is that the mathematical result is based on an idealized model, and many factors that affect the axial deployment force have been ignored, such as the friction between hinges and the assembly error of the actual coilable mast. Even so, the results are still close, with absolute values of relative errors less than 5%, as shown in Equation (11).

Table 2: Axial deployment force results in phase B.

Method	Value range (N)	Average value (N)
Numerical	—	11.808
Simulation	9.606~12.554	11.28
Test	9.592~14.351	11.336

$$\begin{aligned}\text{Simulatation result}: \frac{11.280-11.808}{11.808}\times 100\% = -4.5\%,\\ \text{Test result}: \frac{11.336-11.808}{11.808}\times 100\% = -4.0\%.\end{aligned} \tag{11}$$

5. Conclusion

In this paper, a numerical method for determining the axial deployment force of a coilable mast in practice is presented. According to the "standard shape" in the transition zone of the coilable mast in the local coil mode, the calculation process of the complex axial deployment force is transformed into the solution of the lanyard tension, which is obtained by analysing the deformation of the longeron in the transition zone. To verify the correctness and applicability of the proposed numerical method, dynamic simulation and microgravity deployment tests are carried out. The results show that the maximum relative error is less than 5%. The verified method can be used to easily obtain the estimated axial deployment force of the coilable mast in the local coil mode without complicated simulations and testing, which provides convenience for the design of the coilable mast.

Data Availability

The data used to support the findings of this study are included within the article.

Disclosure

The manuscript is new, neither the entire paper nor any part of its content has been published or accepted elsewhere, and it is not currently under consideration or review by any other journal.

Conflicts of Interest

There is no conflict of interest in the manuscript.

References

[1] L. Puig, A. Barton, and N. Rando, "A review on large deployable structures for astrophysics missions," *Acta Astronautica*, vol. 67, pp. 12–26, 2010.

[2] F. A. Harrison, W. W. Craig, F. E. Christensen et al., "The nuclear spectroscopic telescope array (NuSTAR) high-energy X-ray mission," *The Astrophysical Journal*, vol. 770, no. 2, p. 103, 2013.

[3] Y. Sato, S. K. Kim, Y. Kusakawa et al., "Extensible flexible optical system for nano-scale remote sensing satellite "PRISM"," *Transactions of the Japan Society for Aeronautical and Space Sciences, Space Technology Japan*, vol. 7, no. 26, pp. 13–18, 2008.

[4] L. Johnson, L. Alexander, L. Fabisinski et al., "Multiple NEO rendezvous using solar sail propulsion," in *Global Space Exploration Conference*, Washington, DC, 2012.

[5] M. E. McEachen, "Validation of SAILMAST technology and modeling by ground testing of a full-scale flight article," in *The 48th AIAA Aerospace Sciences Meeting Including the New Horizons Forum and Aerospace Exposition*, Orlando, Florida, 2010.

[6] D. M. Murphy, M. E. McEachen, and B. D. Macy, "Demonstration of a 20-m solar sail system," in *The 46th AIAA/ASME/ASCE/AHS/ASC Structures, Structural Dynamics and Materials Conference*, Austin, Texas, 2005.

[7] M. Natori, K. Okazaki, M. Sakamaki, M. Tabata, and K. Miura, "Model study of simplex masts," in *Proceedings of International Symposium on Space Technology and Science*, pp. 489–496, Tokyo, Japan, 1986.

[8] T. Kitamura, K. Okazaki, M. Natori, K. Miura, S. Sato, and A. Obata, "Development of a "hingeless mast" and its applications," *Acta Astronautica*, vol. 17, pp. 341–346, 1998.

[9] W. Seemann, "Deformation of an elastic helix in contact with a rigid cylinder," *Archive of Applied Mechanics*, vol. 67, pp. 117–139, 1996.

[10] G. H. M. Van Der Heijden, "The static deformation of a twisted elastic rod constrained to lie on a cylinder," *Proceedings of the Royal Society A*, vol. 457, pp. 695–715, 2001.

[11] L. Yanzhu, *Nonlinear Mechanics of Thin Elastic Rod: Theoretical Basis of Mechanical Model of DNA*, Tsinghua University Press, 2006.

[12] H. Jianbin, X. Wang, and H. Ma, "Mechanical principle of the deploying mode for coilable mast," *Journal of Beijing University of Aeronautics and Astronautics*, vol. 39, pp. 1168–1173, 2013.

[13] M. Haibo, H. Hai, H. Jianbing, Z. Wei, and W. Xinsheng, "Study on the criterion to determine the bottom deployment modes of a coilable mast," *Acta Astronautica*, vol. 141, pp. 89–97, 2017.

[14] O. Tutsoy, K. Balikci, and N. F. Ozdil, "Unknown uncertainties in the COVID-19 pandemic: multi-dimensional identification and mathematical modelling for the analysis and estimation of the casualties," *Digital Signal Processing*, vol. 114, article 103058, 2021.

[15] H. Ma, "Triangle-section coilable mast development for BUAA-SAT," in *65th International Astronautical Congress*, Toronto, Canada, 2014.

[16] M. Eiden, O. Brunner, and C. Stavrinidis, "Deployment analysis of the Olympus Astromast and comparison with test measurements," *Journal of Spacecraft and Rockets*, vol. 24, pp. 63–68, 1987.